K. Rajanikanth2026, 14:2
ISSN (Online): 2348-4098
ISSN (Print): 2395-4752

International Journal of Science, Engineering and Technology
An Open Access Journal

Peristaltic Transport of a Newtonian Fluid in an Asymmetric Channel with Wall Slip: Influence of Waveform Shapes

K. Rajanikanth
Department of Mathematics, SRR & CVR GDC (A), Vijayawada, 520004, AP, India

Abstract- This study investigates the effects of wall slip and various waveforms on the peristaltic transport of a Newtonian fluid in a two-dimensional asymmetric channel. Channel asymmetry is generated by imposing peristaltic wave trains of different amplitudes and phase differences on the upper and lower channel walls. The mathematical formulation is developed under the assumptions of long wavelength and low Reynolds number. Exact analytical solutions for the stream function, axial velocity, and pressure gradient are obtained. Numerical computations are performed to analyze pumping characteristics, frictional forces, trapping, and reflux phenomena. Results show that increasing the permeability parameter reduces pumping against pressure rise, axial velocity, pressure gradient, trapped bolus size, and reflux layer thickness. For sufficiently large permeability, symmetry of the trapped bolus is lost. Under certain conditions, closed streamlines form, resulting in trapped boluses moving with the wave speed. A comparative analysis of four waveforms—triangular, sinusoidal, trapezoidal, and square—indicates that the square waveform yields the highest volumetric flux.

Keywords: Peristaltic transport; wall slip; pumping; trapping; reflux; waveforms

I. INTRODUCTION

Peristaltic motion serves as a primary mechanism for fluid transport in biological systems, driven by progressive waves of contraction and relaxation along flexible tubes or channels. This process facilitates transport in physiological contexts, including the esophagus, gastrointestinal tract, stomach, cervical canal, ureter, fallopian tubes, and small intestine. Beyond biology, peristaltic pumping is essential in industrial and biomedical devices such as roller pumps, finger pumps, and food-processing equipment.

The foundational analysis of peristaltic transport was presented by Latham [1]. Subsequent developments by Jaffrin and Shapiro [2] and Jaffrin [3] established key mathematical frameworks for peristaltic pumping. Numerous subsequent investigations have explored two-dimensional symmetric and asymmetric channels under periodic sinusoidal waves [4–11], elucidating critical phenomena such as pumping, trapping, and reflux. Analytical approaches typically include small-amplitude perturbations for arbitrary Reynolds numbers or lubrication approximations that neglect inertial and curvature effects. Both methodologies have been corroborated through experimental and numerical validations.

Wall slip effects have garnered significant interest owing to their relevance in biomedical and engineering applications, including blood dialysis, oxygenators, gaseous diffusion, transpiration cooling, and capillary blood flow. The pioneering slip boundary condition was proposed by Beavers and Joseph [12] and later refined by Saffman [13]. Recent studies have incorporated slip alongside fluid rheology, channel asymmetry, wave propagation, and related factors in peristaltic models [14–23].

The present study builds upon this foundation by examining the peristaltic transport of a Newtonian fluid in an asymmetric channel with wall slip, adopting the geometric setup introduced by Hayat et al. [23]. Particular emphasis is placed on the combined influence of the slip (permeability) parameter and waveform shape (triangular,

sinusoidal, trapezoidal, and square) on key flow characteristics, including pumping performance, pressure gradient, velocity profiles, trapping, and reflux.

Ongoing research continues to address peristaltic transport under increasingly complex conditions, such as asymmetry, slip, electromagnetic fields, and non-Newtonian rheology. For instance, Magdy et al. [24] analyzed the interplay of slip, heat transfer, and magnetohydrodynamic (MHD) effects on peristaltic flow in an asymmetrically inclined channel, revealing significant interactions between slip and MHD on pressure and velocity fields. Investigations into thermal and viscous slip in peristaltic nanofluid transport with microorganisms in porous media have underscored the role of slip in augmenting heat transfer and flow behavior. Ellahi et al. [25] developed an electroosmotic slip flow model for non-Newtonian third-grade MHD fluids using response surface methodology, demonstrating high parameter sensitivity in the resulting flow dynamics. Additionally, a detailed theoretical study of peristaltic pumping in porous conduits [26] highlighted how wall permeability markedly influences flow direction and recirculation patterns, with implications for biological and environmental systems.

This work extends prior analyses by providing exact analytical solutions under long-wavelength and low-Reynolds-number assumptions, with a systematic comparison of multiple waveforms—offering new insights into optimizing peristaltic performance in asymmetric configurations with slip.

II. MATHEMATICAL FORMULATION AND SOLUTION

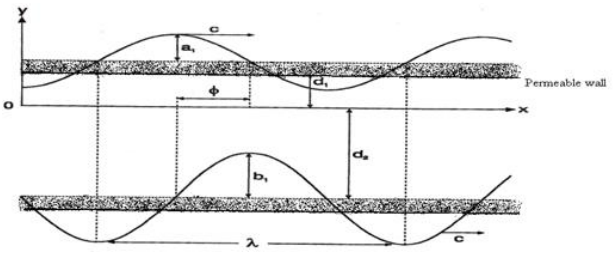

Figure 1. Schematic diagram of a two-dimensional asymmetric channel

We consider the motion of an incompressible viscous fluid in a two-dimensional asymmetric channel (Fig. 1). Sinusoidal wave trains propagate with constant speed along the channel walls.

$$\bar{Y} = H_1 = \bar{d}_1 + \bar{a}_1 \cos\left[\frac{2\pi}{\lambda}\left(\bar{X} - c\bar{t}\right)\right] \text{.....upper wall,} \quad (1)$$

$$\bar{Y} = H_2 = -\bar{d}_2 - \bar{b}_1 \cos\left[\frac{2\pi}{\lambda}(\bar{X} - c\bar{t}) + \phi\right] \text{.....lower wall.} \quad (2)$$

where $\bar{a}_1$ and $\bar{b}_1$ are the amplitudes of the waves, λ is the wave length, $\bar{d}_1 + \bar{d}_2$ is the width of the channel, c is the velocity of propagation, $\bar{t}$ is the time and $\bar{X}$ is the direction of wave propagation. The phase difference ϕ varies in the range $0 \le \phi \le \pi$ in which $\phi = 0$ corresponds to symmetric channel with waves out of phase and $\phi = \pi$ the waves are in phase. Further $\bar{a}_1,\ \bar{b}_1,\ \bar{d}_1,\ \bar{d}_2$ and ϕ satisfy the condition $\bar{a}_1^2 + \bar{b}_1^2 + 2\bar{a}_1\bar{b}_1 \cos\phi \le (\bar{d}_1 + \bar{d}_2)^2$.

The governing equations of motion are given by

$$\frac{\partial \bar{U}}{\partial \bar{X}} + \frac{\partial \bar{V}}{\partial \bar{Y}} = 0, \quad (3)$$

$$\frac{\partial \bar{U}}{\partial \bar{t}} + \bar{U}\frac{\partial \bar{U}}{\partial \bar{X}} + \bar{V}\frac{\partial \bar{U}}{\partial \bar{Y}} = -\frac{1}{\rho}\frac{\partial \bar{P}}{\partial \bar{X}} + \nu\left(\frac{\partial^2 \bar{U}}{\partial \bar{X}^2} + \frac{\partial^2 \bar{U}}{\partial \bar{Y}^2}\right), \quad (4)$$

$$\frac{\partial \bar{V}}{\partial \bar{t}} + \bar{U}\frac{\partial \bar{V}}{\partial \bar{X}} + \bar{V}\frac{\partial \bar{V}}{\partial \bar{Y}} = -\frac{1}{\rho}\frac{\partial \bar{P}}{\partial \bar{Y}} + \nu\left(\frac{\partial^2 \bar{V}}{\partial \bar{X}^2} + \frac{\partial^2 \bar{V}}{\partial \bar{Y}^2}\right), \quad (5)$$

where $\bar{U}$ and $\bar{V}$ are the respective velocity components in the $\bar{X}$ and $\bar{Y}$ directions in the fixed frame, $\bar{P}$ is the fluid pressure, ρ is the constant density of the fluid and ν is the kinematic viscosity.

We introduce a wave frame $(\bar{x},\bar{y})$ moving with velocity c away from the fixed frame $(\bar{X},\bar{Y})$ by the transformations

$$\bar{x}=\bar{X}-c\bar{t},\ \bar{y}=\bar{Y},\ \bar{u}=\bar{U}-c,\ \bar{v}=\bar{V},\quad \bar{p}(x)=\bar{P}(X,t)$$
. (6)

The appropriate non-dimensional variables and parameters are defined as

$$x=\frac{\bar{x}}{\lambda},y=\frac{\bar{y}}{\bar{d}_1},\ u=\frac{\bar{u}}{c},\ v=\frac{\bar{v}}{c},\ h_1=\frac{H_1}{\bar{d}_1},$$

$$h_2=\frac{H_2}{\bar{d}_2},\ \ t=\frac{c}{\lambda}\bar{t},\ a=\frac{\bar{a}_1}{\bar{d}_1},\ b=\frac{\bar{b}_1}{\bar{d}_1},\ d=\frac{\bar{d}_2}{\bar{d}_1},$$

$$\delta=\frac{\bar{d}_1}{\lambda},\ v=\frac{\bar{V}}{c\delta},\ R_e=\frac{c\bar{d}_1}{\nu},\ \psi=\frac{\bar{\psi}}{c\bar{d}_1},\ Da=\frac{k}{d_1^2}.$$

Using the above non-dimensional variables and parameters Eqs. (3) - (5) in terms of stream function $\psi\left(u=\frac{\partial\psi}{\partial y},v=-\delta\frac{\partial\psi}{\partial x}\right)$ is given by

$$R_e\delta\left\{\psi_y\psi_{yyx}-\psi_x\psi_{yyy}+\delta^2\left(\psi_y\psi_{xxx}-\psi_x\psi_{xxy}\right)\right\}=\psi_{yyyy}+2\delta^2\psi_{xxyy}+\delta^4\psi_{xxxx}$$
. (7)

Here and in what follows the subscripts x and y denote the partial differentiations.

The corresponding boundary conditions in terms of stream function ψ are defined as

$$\psi=\frac{q}{2}\ at\ y=h_1(x),$$
(8)

$$\psi=\frac{-q}{2}\ at\ y=h_2(x),$$
(9)

$$\frac{\partial\psi}{\partial y}+\beta\frac{\partial^2\psi}{\partial y^2}=-1\ at\ y=h_1(x),$$
(10)

$$\frac{\partial\psi}{\partial y}-\beta\frac{\partial^2\psi}{\partial y^2}=-1\ at\ y=h_2(x),$$
(11)

with

$$h_1(x)=1+a\cos 2\pi x,$$

$$h_2(x)=-d-b\cos(2\pi x+\phi).$$

where q is the flux in fixed frame and a, b, d and ϕ satisfy the relation $a^2+b^2+2ab\cos\phi\le(1+d)^2$.

Under the assumptions of the long wavelength $\delta<<1$ and low Reynolds number, the Eq. (7) becomes

$$\psi_{yyyy}=0.$$
(12)

The solution of Eq. (12) satisfying the corresponding boundary conditions (8) to (11) is

$$\psi=\frac{(q+h_1-h_2)}{(h_1-h_2)^2(h_1-h_2-6\beta)}\left(2y^3-3(h_1+h_2)y^2-6(h_1-h_2-h_1h_2)y+6\beta h_1(h_1-h_2)-h_1^3+3h_1^2h_2\right)$$

$$+\frac{q}{2}+h_1-y,$$
(13)

$$u=\frac{6(q+h_1-h_2)}{(h_1-h_2)^2(h_2-h_1-6\beta)}\left(y^2-(h_1+h_2)y-h_1+h_2+h_1h_2\right)-1$$
. (14)

For $h_2\le y\le h_1$ the flux at any axial station in the fixed frame is

$$Q=\int_{h_2}^{h_1}(u+1)dy=\int_{h_2}^{h_1}udy+\int_{h_2}^{h_1}dy=q+(h_1+h_2)\cdot$$

(15)

The average volume flow rate over one period $\left(T=\frac{\lambda}{c}\right)$ of the peristaltic wave is defined as

$$\overline{Q}=\frac{1}{T}\int_{o}^{T}(q+(h_1-h_2)dt=q+1+d\cdot$$

(16)

The pressure gradient is obtained from the dimensionless momentum equation for the axial velocity $\frac{dp}{dx}=\psi_{yyy}$ and substituting for ψ from (13), we get

$$\frac{dp}{dx}=\frac{12\left(q+h_1-h_2\right)}{\left(h_1-h_2\right)^2\left(h_2-h_1-6\beta\right)}.$$

(17)

Integrating equation (17) over wavelength one obtains

$$\Delta p_L=\int_0^L\left(\frac{dp}{dx}\right)dx=p_L-p_0\cdot$$

(18)

The integral in (18) will be independent of time only when L is an integral multiple of λ. In this problem either we have to prescribe Δp or $\overline{Q}$ and by prescribing either Δp or $\overline{Q}$ as constants, the flow can be treated as steady. The integral in (18) is evaluated over one wavelength using the values of the integrals given in Appendix and replacing q with $\overline{Q}$ from (16). Finally are have

$$\Delta p=\frac{\left(q-6\beta\right)}{3\beta^2\left((1+d)^2-(a^2+b^2+2ab\cos\phi)\right)^{\frac{1}{2}}}-\frac{2q(1+d)^2}{\beta\left((1+d)^2-(a^2+b^2+2ab\cos\phi)\right)^{\frac{3}{2}}}$$

$$+\frac{\left(q-6\beta\right)}{3\beta^2\left((1+d+6\beta)^2-(a^2+b^2+2ab\cos\phi)\right)^{\frac{1}{2}}}\quad.$$

(19)

The above expression may be rewritten as

$$\overline{Q}=\frac{\left[\begin{array}{l}3\beta\left((1+d+6\beta)^2-(a^2+b^2+2ab\cos\phi)\right)^{\frac{1}{2}}\left(\Delta p\beta\left((1+d)^2-(a^2+b^2+2ab\cos\phi)\right)^{\frac{3}{2}}-2\right)\\+\left(\left((1+d)^2-(a^2+b^2+2ab\cos\phi)\right)\left((1+d+6\beta)^2-(a^2+b^2+2ab\cos\phi)\right)^{\frac{1}{2}}\right.\\\left.-\left((1+d)^2-(a^2+b^2+2ab\cos\phi)\right)^{\frac{3}{2}}\right)(6\beta+1+d)\end{array}\right]}{\left[\begin{array}{l}\left((1+d+6\beta)^2-(a^2+b^2+2ab\cos\phi)\right)^{\frac{1}{2}}\left(\left((1+d)^2-(a^2+b^2+2ab\cos\phi)\right)-6\beta\right)\\-\left((1+d)^2-(a^2+b^2+2ab\cos\phi)\right)^{\frac{3}{2}}\end{array}\right]}$$

. (20)

The results for the corresponding symmetric channel can be obtained from our results by putting $a=b$, $d=1$ and $\phi=0$. Eq. (20) reduces to Poiseuille law for a channel when $\Delta p<0$, $a=b=0$ channel with straight walls or $a=b$ and $\phi=\pi$ a channel with peristaltic waves with same amplitude and in phase.

The frictional forces at y= h_1 and y= h_2 are denoted by

$$F_1=\int_0^1-h_1^2\left(\frac{dp}{dx}\right)dx,$$

(21)

$$F_2=\int_0^1-h_2^2\left(\frac{dp}{dx}\right)dx\cdot$$

(22)

III. EXPRESSIONS FOR WAVE SHAPE

The non-dimensional expressions for the four waveforms considered in this study are:

Triangular wave:

$$h_1(x)=1+a\left\{\frac{8}{\pi^3}\sum_{m=1}^{\infty}\frac{(-1)^{m+1}}{(2m-1)^2}\sin[(2m-1)x]\right\},$$

(23)

$$h_2(x)=-d-b\left\{\frac{8}{\pi^3}\sum_{m=1}^{\infty}\frac{(-1)^{m+1}}{(2m-1)^2}\sin[(2m-1)x+\phi]\right\}.$$

(24)

Sinusoidal wave:

$$h_1(x)=1+a\sin(x),$$

(25)

$$h_2(x)=-d-b\sin(x+\phi).$$

(26)

Trapezoidal wave:

$$h_1(x)=1+a\left\{\frac{32}{\pi^2}\sum_{m=1}^{\infty}\frac{\sin\frac{\pi}{8}(2m-1)}{(2m-1)^2}\sin[(2m-1)x]\right\},$$

(27)

$$h_2(x)=-d-b\left\{\frac{32}{\pi^2}\sum_{m=1}^{\infty}\frac{\sin\frac{\pi}{8}(2m-1)}{(2m-1)^2}\sin[(2m-1)x+\phi]\right\}$$

. (28)

Square wave:

$$h_1(x)=1+a\left\{\frac{4}{\pi}\sum_{m=1}^{\infty}\frac{(-1)^{m+1}}{(2m-1)}\cos\left[(2m-1)x\right]\right\}$$

, (29)

$$h_2(x)=-d-b\left\{\frac{4}{\pi}\sum_{m=1}^{\infty}\frac{(-1)^{m+1}}{(2m-1)}\cos\left[(2m-1)x+\phi\right]\right\}.$$

(30)

IV. DISCUSSION OF THE RESULTS

Pumping Characteristics

Peristaltic motion is characterized by the ability to pump fluid against an adverse pressure gradient. From Eq. (20), the following conditions arise:

- For ΔP>0, pumping occurs against a pressure rise.
- For ΔP=0, free pumping occurs.
- For ΔP<0, the flow is assisted by pressure (co-pumping).

A critical flux value exists below which peristaltic pumping occurs and above which augmented pumping is observed. Figures 2 and 3 illustrate the variation of pressure rise with time-averaged flux for different slip and permeability parameters.

Increasing slip decreases the free-pumping flux, indicating that wall slip reduces the effective peristaltic pumping region. Similarly, increasing permeability widens the pumping region, shifting the system toward augmented pumping. These findings are consistent with earlier literature [5].

$$\Delta p_{max}=\frac{\left[\begin{array}{l}\left((1+d)^2-(a^2+b^2+2ab\cos\phi)\right)^{\frac{3}{2}}\left(6\beta+1+d\right)+6\beta\left((1+d+6\beta)^2-(a^2+b^2+2ab\cos\phi)\right)^{\frac{1}{2}}\\-\left((1+d)^2-(a^2+b^2+2ab\cos\phi)\right)\left((1+d+6\beta)^2-(a^2+b^2+2ab\cos\phi)\right)^{\frac{1}{2}}\end{array}\right]}{3\beta^2\left((1+d+6\beta)^2-(a^2+b^2+2ab\cos\phi)\right)^{\frac{1}{2}}\left((1+d)^2-(a^2+b^2+2ab\cos\phi)\right)^{\frac{3}{2}}}$$

(31)

$$\bar{Q}_{max}=\frac{\left[\begin{array}{l}\left(6\beta+1+d\right)\left(\left((1+d)^2-(a^2+b^2+2ab\cos\phi)\right)\left((1+d+6\beta)^2-(a^2+b^2+2ab\cos\phi)\right)^{\frac{1}{2}}\right.\\\left.-\left((1+d)^2-(a^2+b^2+2ab\cos\phi)\right)^{\frac{3}{2}}\right)-6\beta\left((1+d+6\beta)^2-(a^2+b^2+2ab\cos\phi)\right)^{\frac{1}{2}}\end{array}\right]}{\left[\begin{array}{l}\left((1+d+6\beta)^2-(a^2+b^2+2ab\cos\phi)\right)^{\frac{1}{2}}\left(\left((1+d)^2-(a^2+b^2+2ab\cos\phi)\right)-6\beta\right)\\-\left((1+d)^2-(a^2+b^2+2ab\cos\phi)\right)^{\frac{3}{2}}\end{array}\right]}$$

. (32)

Velocity distribution and pressure gradient

The maximum velocity occurs at $y=\frac{h_1+h_2}{2}$.

From Eq. (14) are obtain

$$u_{max}=\frac{3\left(1+d-\overline{Q}\right)\left(h_2-h_1\right)\left(4-h_2+h_1\right)+\left(h_1-h_2\right)^2\left(12\left(\beta-1\right)-h_1+h_2\right)}{2\left(h_1-h_2\right)^2\left(h_2-h_1-6\beta\right)}$$

. (33)

Figure 7 shows that increasing slip parameter increases velocity near the walls but decreases it near the centerline. The pressure gradient decreases with increasing slip, permeability, mean flux, and phase shift (Fig. 8).

Trapping criterion

It has been shown in [3] that under certain conditions, the streamlines $\psi=0$ at the central line split to enclose a bolus of fluid particles circulating along closed streamline. This bolus moves at the wave velocity and therefore appears to be trapped by the wave. A criterion for the presence of trapping is the existence of stagnation points in the wave frame which are located at the intersection of the curve $\psi=0$ and the central line.

The axial velocity component at the centre line is obtained by setting $y=0$ in the Eq. (14) and the stagnation points are given by

$$u(x,0)=\frac{6\left(1+d-\overline{Q}+h_1(x)-h_2(x)\right)\left(h_1(x)-h_2(x)+h_1(x)h_2(x)\right)+\left(h_1(x)-h_2(x)\right)^3-6\beta\left(h_1(x)-h_2(x)\right)^2}{\left(h_1(x)-h_2(x)\right)^2\left(h_2(x)-h_1(x)-6\beta\right)}$$

. (34)

Trapping occurs when closed streamlines surround a bolus of fluid moving with the wave. Stagnation points satisfy Eq. (34), and streamline plots (Figs. 9–13) show that:

- Trapping bolus size increases with mean flux.
- It decreases with increasing slip.
- Increasing phase shift shifts bolus location and reduces its size.
- Square waves yield the largest trapped boluses, consistent with their higher flux.

Reflux Criterion

It has been shown in the studies [3, 5] that under certain condition the fluid particles near the walls have a mean speed of advance opposite to the main flow. This phenomenon may explain the ureteral reflux named after the observation that bacteria sometimes travel from the bladder to the kidneys in opposite direction to the main urine flow.

$$\frac{\overline{Q}}{\overline{Q}_{max}}=\frac{\left[\begin{array}{l}3\beta\left(\left(1+d+6\beta\right)^2-\left(a^2+b^2+2ab\cos\phi\right)\right)^{\frac{1}{2}}\left(\Delta p\beta\left(\left(1+d\right)^2-\left(a^2+b^2+2ab\cos\phi\right)\right)^{\frac{3}{2}}-2\right)\\+\left(\left(\left(1+d\right)^2-\left(a^2+b^2+2ab\cos\phi\right)\right)\left(\left(1+d+6\beta\right)^2-\left(a^2+b^2+2ab\cos\phi\right)\right)^{\frac{1}{2}}\right.\\\left.-\left(\left(1+d\right)^2-\left(a^2+b^2+2ab\cos\phi\right)\right)^{\frac{3}{2}}\right)\left(6\beta+1+d\right)\end{array}\right]}{\left[\begin{array}{l}\left(6\beta+1+d\right)\left(\left(\left(1+d\right)^2-\left(a^2+b^2+2ab\cos\phi\right)\right)\left(\left(1+d+6\beta\right)^2-\left(a^2+b^2+2ab\cos\phi\right)\right)^{\frac{1}{2}}\right.\\\left.-\left(\left(1+d\right)^2-\left(a^2+b^2+2ab\cos\phi\right)\right)^{\frac{3}{2}}\right)-6\beta\left(\left(1+d+6\beta\right)^2-\left(a^2+b^2+2ab\cos\phi\right)\right)^{\frac{1}{2}}\end{array}\right]}$$

.(35)

Reflux occurs when the mean particle velocity near the walls reverses direction. From Eq. (35), reflux zones form near the walls depending on pressure rise, phase shift, and slip.

Figures 14–16 show that:

- Reflux layers enlarge with increasing slip and phase shift.
- Increasing pressure rise may shift reflux between upper and lower walls.
- Permeability modulates both trapping and reflux layers.

V. HIGHLIGHTS

- Exact analytical solutions are obtained for peristaltic flow in an asymmetric channel with wall slip.
- The combined effects of permeability and waveform geometry on pumping, trapping, and reflux are analyzed.

- Square waveforms produce the highest volumetric flow rates and largest trapped boluses.
- Increasing slip reduces pressure rise, axial velocity, and trapping size.
- Results provide insights for biomedical and engineering peristaltic transport systems.

VI. CONCLUSION

A mathematical model for peristaltic transport of a Newtonian fluid in an asymmetric channel with wall slip was developed under long-wavelength and low-Reynolds-number assumptions. Analytical solutions reveal the significant influence of slip, permeability, and waveform shape on pumping, pressure gradient, trapping, and reflux phenomena. Square waveforms yield the highest flux and largest trapping zones. The results align with prior studies and extend understanding of peristaltic transport in physiological systems and engineering devices.

Appendix

$$\int_0^{2\pi} \frac{d\theta}{\alpha+\beta\cos\theta+\gamma\sin\theta} = \frac{2\pi}{\sqrt{\alpha^2-\beta^2-\gamma^2}}, \quad \alpha > \sqrt{\beta^2+\gamma^2}$$

$$\int_0^{2\pi} \frac{d\theta}{(\alpha+\beta\cos\theta+\gamma\sin\theta)^2} = \frac{2\pi\alpha}{(\alpha^2-\beta^2-\gamma^2)^{\frac{3}{2}}},$$

$$\int_0^{2\pi} \frac{d\theta}{(\alpha+\beta\cos\theta+\gamma\sin\theta)^3} = \frac{\pi(2\alpha^2+\beta^2+\gamma^2)}{(\alpha^2-\beta^2-\gamma^2)^{\frac{5}{2}}}.$$

Figures

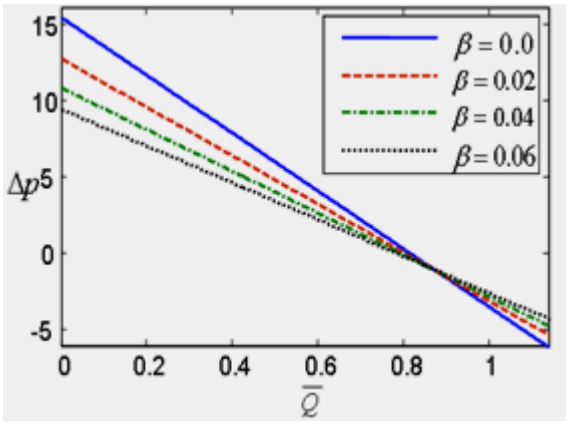

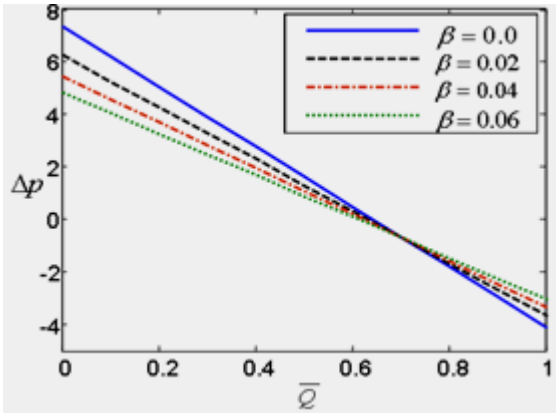

Figure2. The variation of Δp with $\bar{Q}$ and a=0.5, b=0.5, d=0.5, i) $\phi = 0$ and ii) $\phi = \pi/3$.

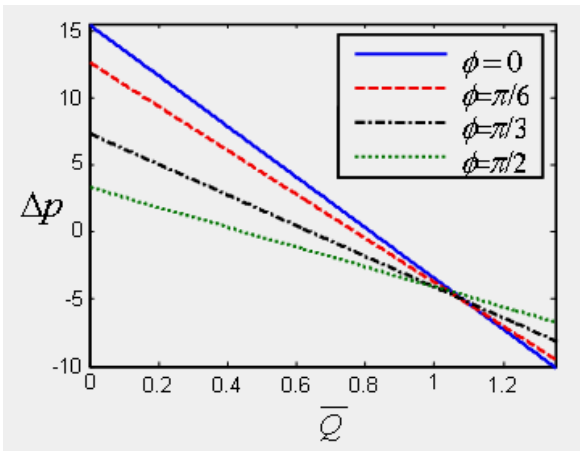

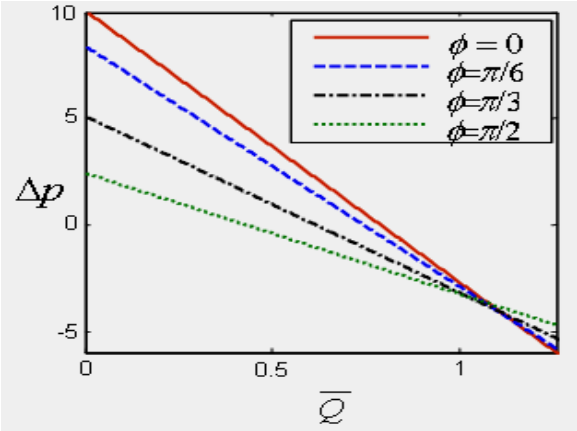

Figure3. The variation of Δp with $\overline{Q}$ and a=0.5, b=0.5, d=0.5, i) $\beta=0$ and ii) $\beta=0.05$.

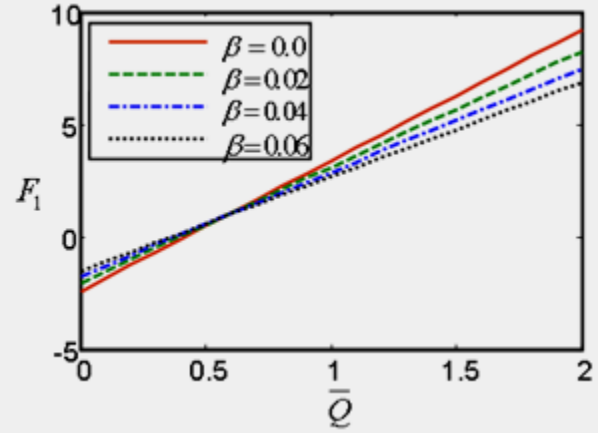

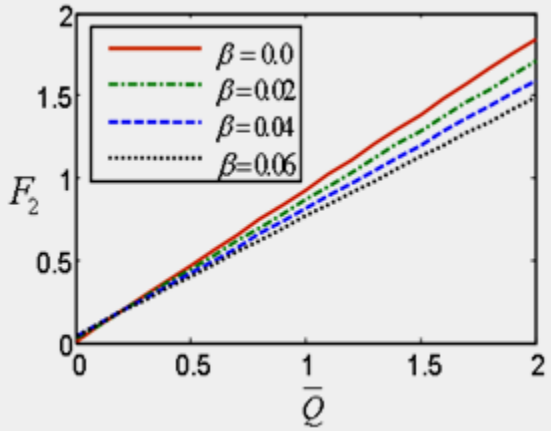

Figure 4. The variation of F_1 and F_2 with $\overline{Q}$ and a=0.5, b=0.5, d=1, $\phi=\pi/3$, i) at $y=h_1$ and ii)at $y=h_2$.

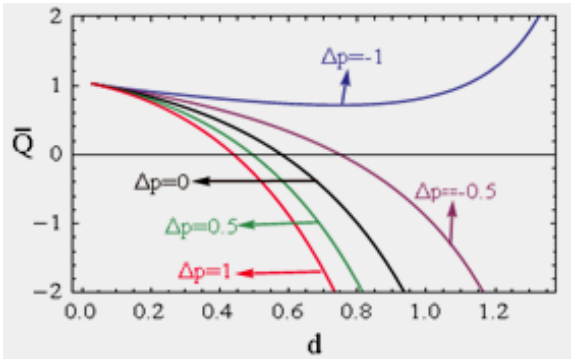

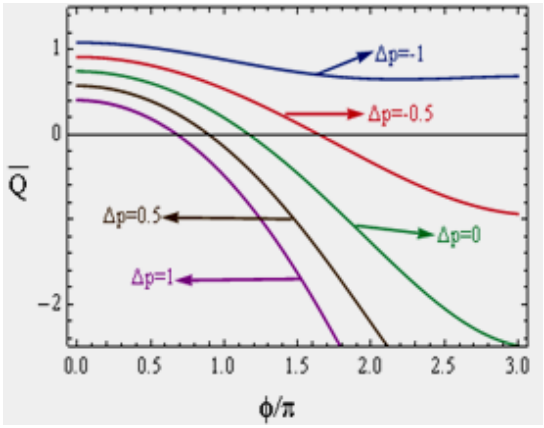

Figure 5. i)The variation of $\overline{Q}$ with d for different Δp with a=0.9, b=0.5, $\phi=\pi/2$ and $\beta=0.6$.

ii) The variation of $\overline{Q}$ with ϕ for different Δp with a=0.8, b=0.6, d=0.7and $\beta=0.5$.

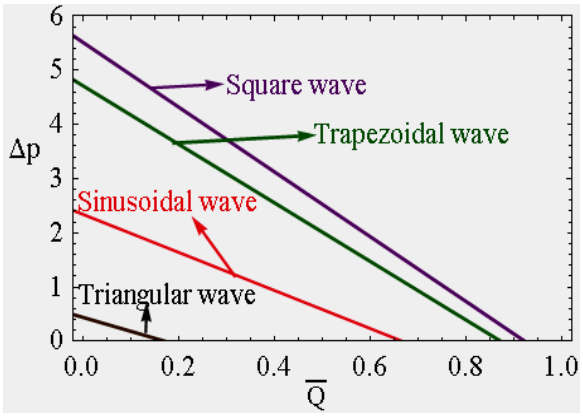

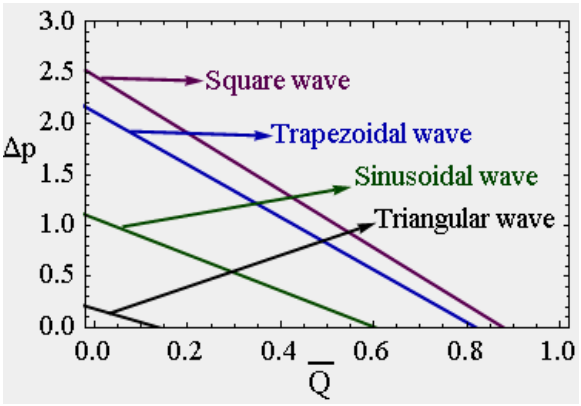

Figure 6. The variation of Δp with $\bar{Q}$ and a=0.5, b=0.5, d=1and $\phi = 0$ i) $\beta = 0$and ii) $\beta = 0.1$.

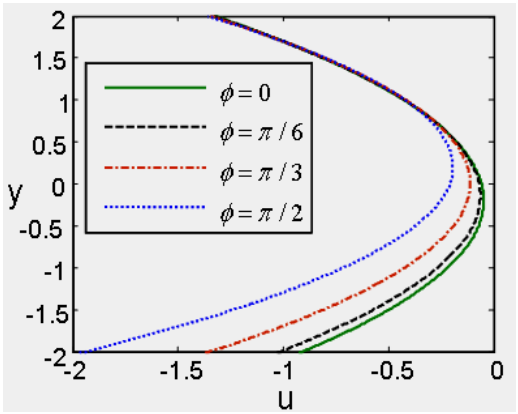

Figure 7. The variation of u with y and a=0.8, b=0.8, d=1 i) $\phi = \pi/3$, $\bar{Q}$=1, ii) $\phi = \pi/3, \beta = 0.5$ and iii) $\beta = 0.5$, $\bar{Q}$=1.

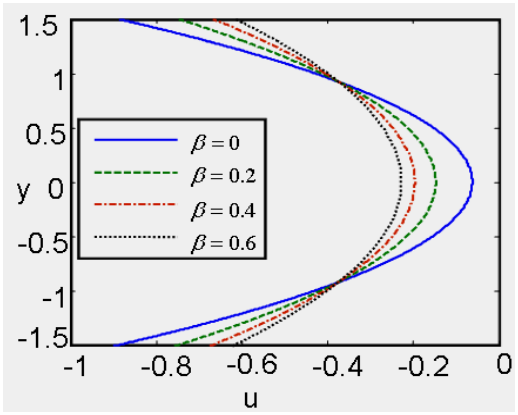

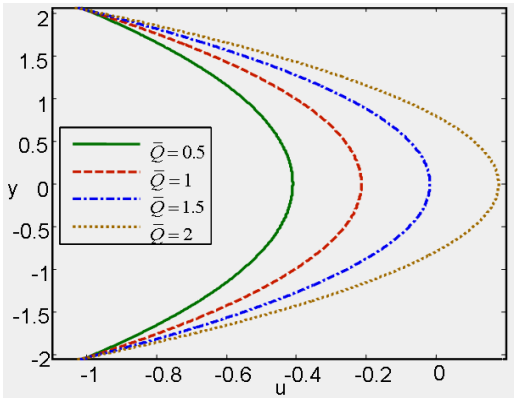

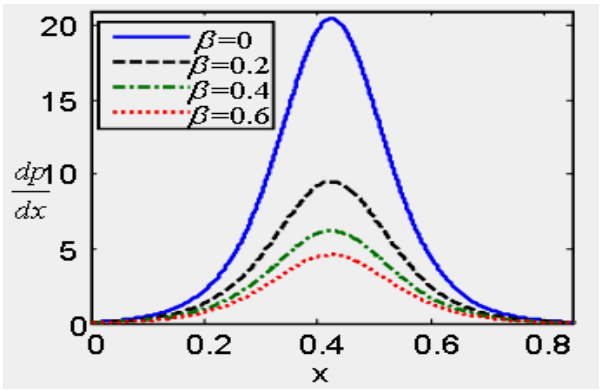

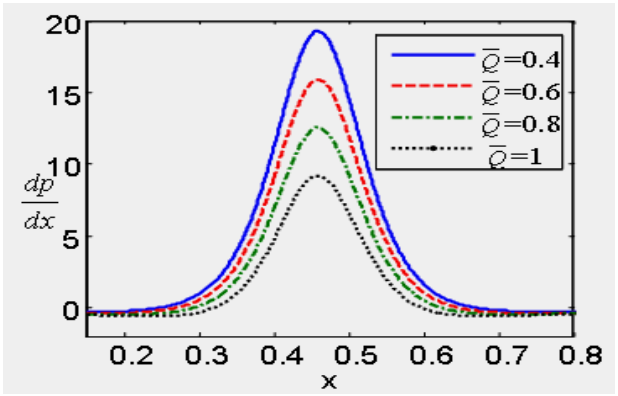

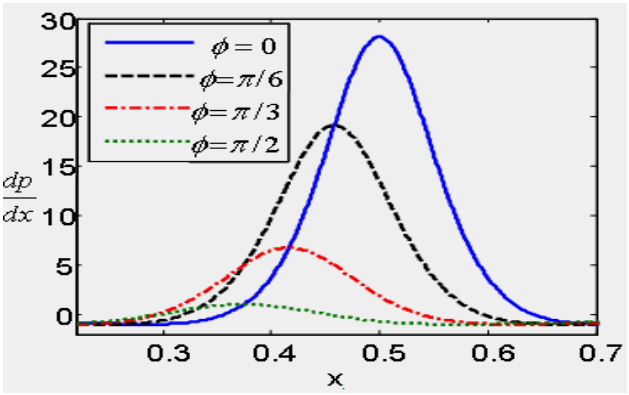

(i) (ii) (iii)

Figure 8. The variation of $\frac{dp}{dx}$ with x and a=0.8, b=0.8, d=1 i) $\phi=\pi/6$, $\bar{Q}$=1, ii) $\beta=0.5, \phi=\pi/6$ and iii) $\beta=0.5$, $\bar{Q}$=1.

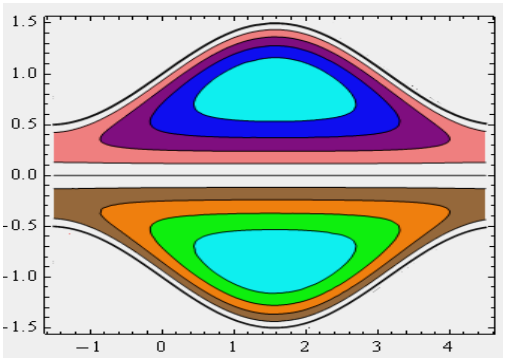

Figure 9. Streamlines for a=0.5, b=0.5, d=1, $\phi=0$, $\beta=0.1$ and for different $\bar{Q}$ i) $\bar{Q}$=1, ii) $\bar{Q}$=1.5 and iii) $\bar{Q}$=2.

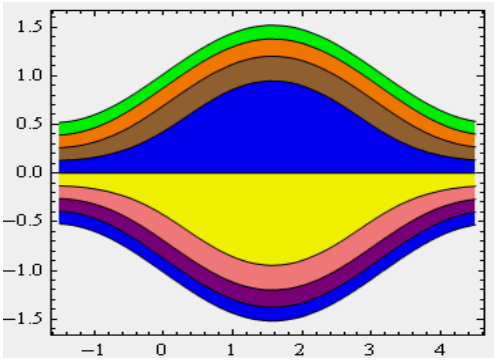

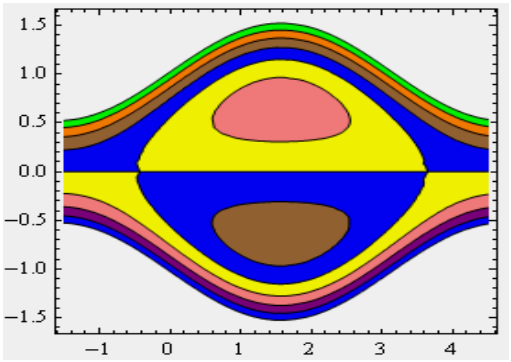

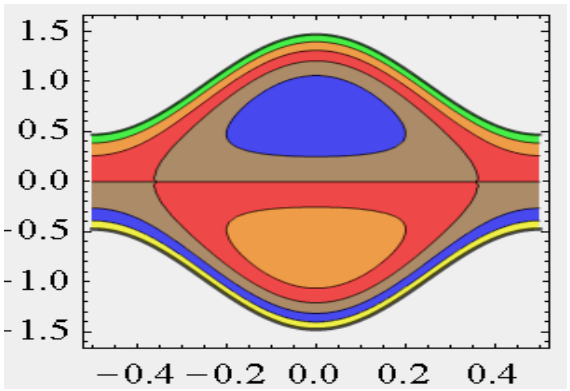

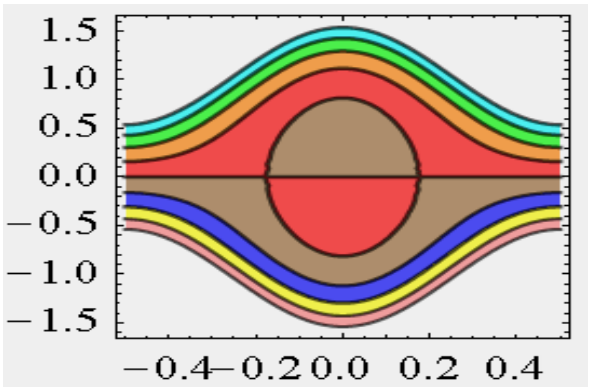

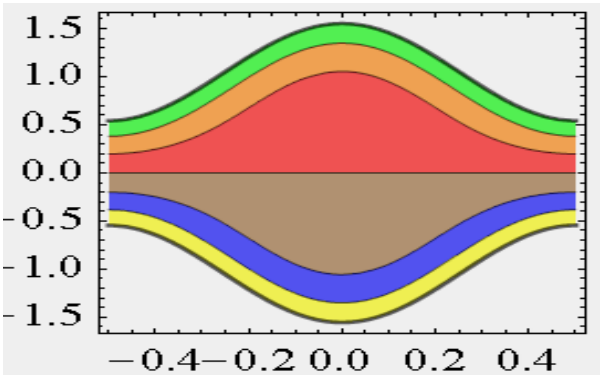

Figure 10. Streamlines for a=0.5, b=0.5, d=1, $\phi=0$, $\bar{Q}$ =1.5 and for different β i) $\beta=0$, ii) $\beta=0.05$ and iii) $\beta=0.08$.

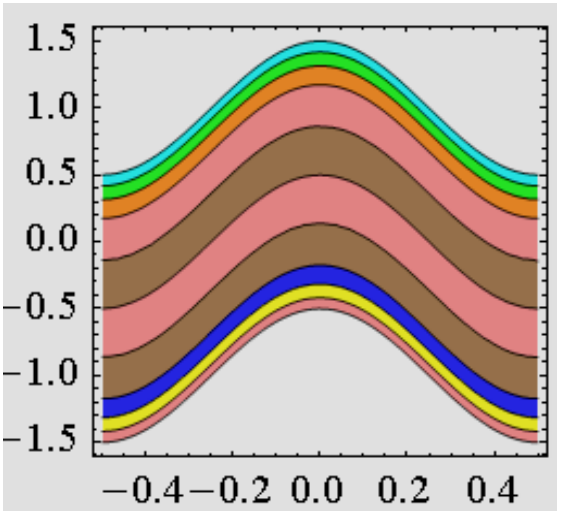

Figure 11. Streamlines for a=0.5, b=0.5, d=1, $\beta=0.1$, $\bar{Q}$ =1.5 and for different ϕ i) $\phi=0$, ii) $\phi=\pi/2$ and iii) $\phi=\pi$

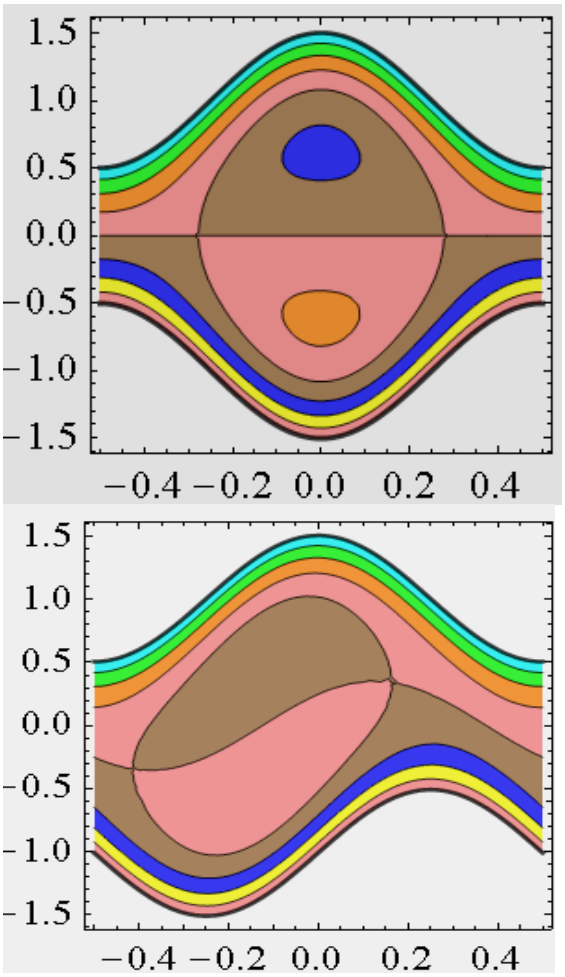

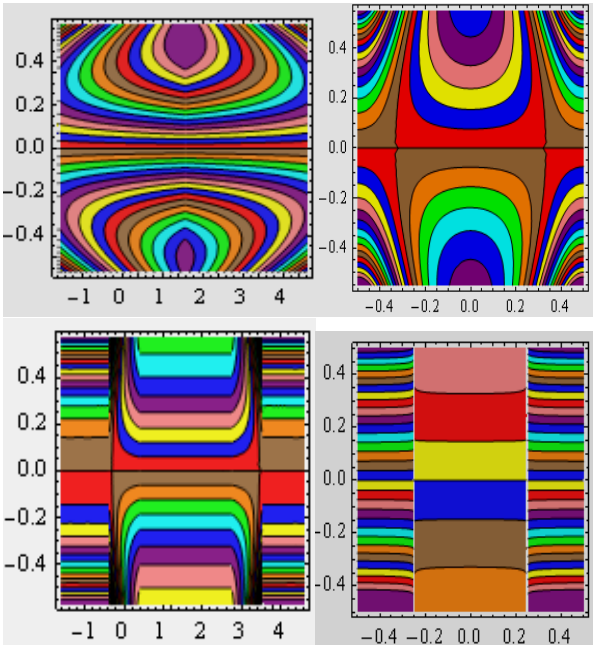

Figure 12. Streamlines for a=0.5, b=0.5, d=1, $\beta=0$, $\phi=0$ $\bar{Q}$=1, i) triangular wave, ii) sinusoidal wave, iii) trapezoidal wave and iv) square wave.

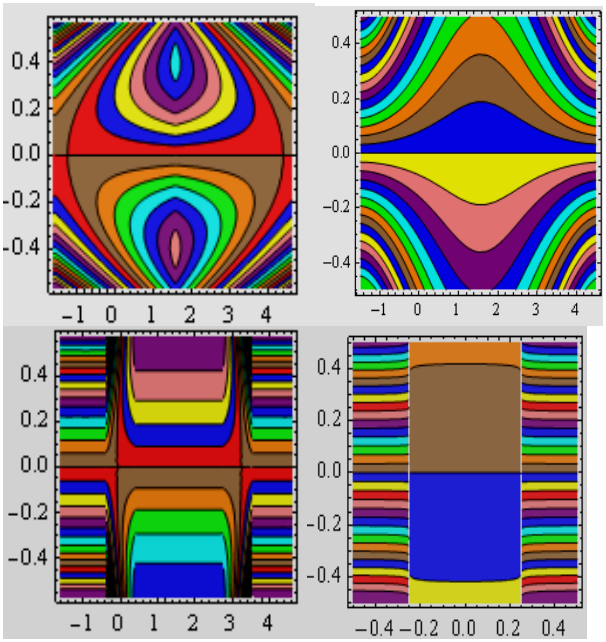

Figure 13. Streamlines for a=0.5, b=0.5, d=1, $\beta=0.1$, $\bar{Q}$ =1, $\phi=0$ i) triangular wave, ii) sinusoidal wave, iii) trapezoidal wave and iv) square wave.

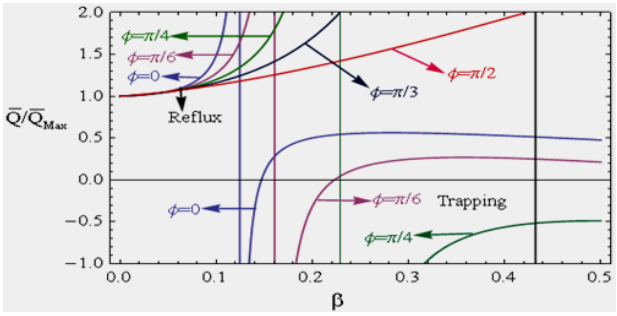

Figure 14. Trapping and reflux limit for different ϕ with a=0.6, b=0.5, d=0.5 and $\Delta p=0.6$.

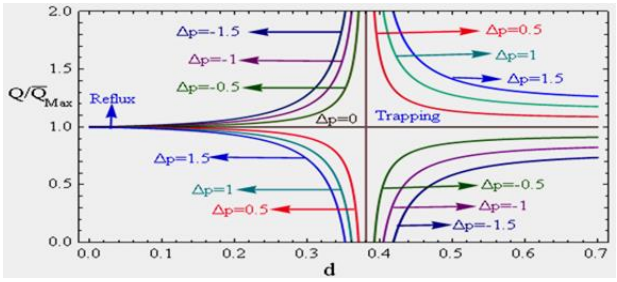

Figure 15. Trapping and reflux limit for different d with a=0.6, b=0.5, $\phi=\pi/6$ and $\beta=0.1$.

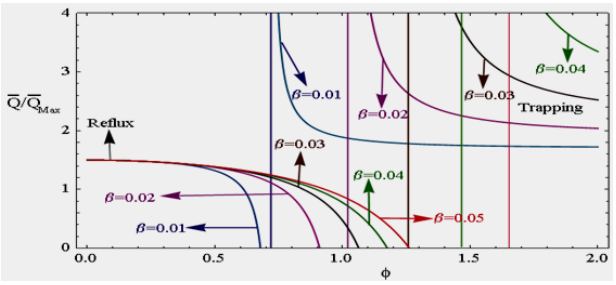

Figure 16. Trapping and reflux limit for different d with a=1, b=0.5, d=0.5 and $\Delta p=0.5$.

Acknowledgement

The author declare that no funds, grants, or other support were received during the preparation of this manuscript

REFERENCES

1. Latham TW (1966) Fluid motions in a peristaltic pump. MS Thesis, Massachusetts Institute of Technology, Cambridge, MA
2. Jaffrin MY, Shapiro AH (1971) Peristaltic pumping. Annu Rev Fluid Mech 3:13–36. https://doi.org/10.1146/annurev.fl.03.010171.000305
3. Jaffrin MY (1973) Inertia and streamline curvature effects on peristaltic pumping. Int J Eng Sci 11:681–699. https://doi.org/10.1016/0020-7225(73)90029-3
4. Shapiro AH, Jaffrin MY, Weinberg SL (1969) Peristaltic pumping with long wavelengths at low Reynolds number. J Fluid Mech 37:799–825. https://doi.org/10.1017/S002211206900089X
5. Mishra M, Ramachandra Rao A (2003) Peristaltic transport of a Newtonian fluid in an asymmetric channel. Z Angew Math Phys 54:532–550. https://doi.org/10.1007/s00033-003-1070-7
6. Pozrikidis C (1987) A study of peristaltic flow. J Fluid Mech 180:515–527. https://doi.org/10.1017/S0022112087001930
7. Radhakrishnamacharya G (1982) Long wavelength approximation to peristaltic motion of a power-law fluid. Rheol Acta 21:30–35. https://doi.org/10.1007/BF01584270
8. Abd El-Naby A, El-Misiery AEM (2002) Effect of an endoscope and generalized Newtonian fluid on peristaltic motion. Appl Math Comput

128:19–35. https://doi.org/10.1016/S0096-3003(01)00057-4
9. Ebaid A (2008) Effects of magnetic field and wall slip condition on the peristaltic transport of a Newtonian fluid in asymmetric channel. Phys Lett A 372:4493–4499. https://doi.org/10.1016/j.physleta.2008.04.038
10. Srivastava LM, Srivastava VP (1985) Peristaltic transport of a non-Newtonian fluid: Applications to the vas deferens and small intestine. Ann Biomed Eng 13:137–153. https://doi.org/10.1007/BF02471166
11. Subba Reddy MV, Ramachandra Rao A, Sreenadh S (2007) Peristaltic motion of a power-law fluid in an asymmetric channel. Int J Non-Linear Mech 42:1153–1161. https://doi.org/10.1016/j.ijnonlinmec.2007.08.003
12. Beavers GS, Joseph DD (1967) Boundary conditions at a naturally permeable wall. J Fluid Mech 30:197–207. https://doi.org/10.1017/S0022112067001375
13. Saffman PG (1971) On the boundary condition at the surface of a porous medium. Stud Appl Math 50:93–101. https://doi.org/10.1002/sapm197150293
14. Vajravelu K, Sreenadh S, Hemadri Reddy K, Murugesan K (2009) Peristaltic transport of a Casson fluid in contact with a Newtonian fluid in a circular tube with wall slip. Int J Fluid Mech Res 36:244–254. https://doi.org/10.1615/InterJFluidMechRes.v36.i3.50
15. Hayat T, Qureshi MU, Hussain Q (2009) Effect of the peristaltic flow of an electrically conducting fluid in a porous space. Appl Math Model 33:1862–1873. https://doi.org/10.1016/j.apm.2008.03.009
16. Elshehaway EF, Eldabe NTM, Ebaid A (2006) Peristaltic transport in an asymmetric channel through a porous medium. Appl Math Comput 182:140–150. https://doi.org/10.1016/j.amc.2006.03.042
17. Kothandapani M, Srinivas S (2008) Nonlinear peristaltic transport in an inclined asymmetric channel through a porous medium. Phys Lett A 372:1265–1276. https://doi.org/10.1016/j.physleta.2007.09.040
18. Mekheimer KhS (2003) Nonlinear peristaltic transport through a porous medium in an inclined planar channel. J Porous Media 6:189–204. https://doi.org/10.1615/JPorMedia.v6.i3.30
19. Misra JC, Pandey SK (2001) A mathematical model for esophageal swallowing of a food-bolus. Math Comput Model 33:997–1009. https://doi.org/10.1016/S0895-7177(00)00300-5
20. Nadeem S, Akbar NS, Bibi N, Ashiq S (2010) Influence of heat and mass transfer on peristaltic flow of a third order fluid in a diverging tube. Commun Nonlinear Sci Numer Simul 15:2916–2931. https://doi.org/10.1016/j.cnsns.2009.11.010
21. Hayat T, Hussain Q, Ali N (2008) Influence of partial slip on the peristaltic flow in a porous medium. Physica A 387:3399–3409. https://doi.org/10.1016/j.physa.2008.02.027
22. Harivaran P, Seshadri V, Rupesh S, Banerjee RK (2008) Peristaltic transport of non-Newtonian fluid in a diverging tube with different wave forms. Math Comput Model 48:998–1017. https://doi.org/10.1016/j.mcm.2007.12.014
23. Hayat T, Ali N, Abbas Z (2008) Peristaltic flow of a micropolar fluid in a channel with different wave forms. Phys Lett A 370:331–344. https://doi.org/10.1016/j.physleta.2007.05.095
24. Magdy M, Nasr AG, Abumandour RM, El-Shorbagy MA (2024) The impact of heat transfer and a magnetic field on peristaltic transport with slipping through an asymmetrically inclined channel. Mathematics 12(12):1827. https://doi.org/10.3390/math12121827
25. Ellahi R, Zeeshan A, Shafique S, Sait SM, Rehman Aur (2025) Electroosmotic slip flow in peristaltic transport of non-Newtonian third-grade MHD fluid: RSM-based sensitivity analysis. Int J Heat Mass Transf 247:127121. https://doi.org/10.1016/j.ijheatmasstransfer.2025.127121
26. Chinnasamy P, Sivajothi R, Sathish S et al (2024) Peristaltic transport of Sutterby nanofluid flow in an inclined tapered channel with an artificial neural network model and biomedical engineering application. Sci Rep 14:555. https://doi.org/10.1038/s41598-023-50955-5